Catal Lett (2011) 141:1219–1227
DOI 10.1007/s10562-011-0618-y

Ethylene Oligomerizations by Diazene Bridged Ni(II) Catalysts Derived from Pyrazole-Scaffold-Based Binucleating Ligands with Alkyl and Aryl Pendant Arms

Srinivasa Budagumpi · Renjith P. Johnson · Hongsuk Suh · Chang-Sik Ha · Il Kim

Received: 10 March 2011 / Accepted: 26 April 2011 / Published online: 7 May 2011

Abstract The coordination and organometallic chemistry of a series of diazene (N_2)-bridged Ni(II) catalysts derived from pyrazole-scaffold-based ligands bearing alkyl and aryl pendent arms was investigated. Binucleating ligands were obtained as products of the condensation reaction between 3,5-dichloroformyl-1H-pyrazole and aliphatic/aromatic primary/secondary amines under anhydrous conditions. The Ni(II) catalysts were activated with ethyl aluminum sesquichloride (EASC) to oligomerize the ethylene mainly into C4, C6, C8, and C10 fractions with activities up to 1.2 and 0.5 $\times$ 10^6 g (mol-Ni)$^{-1}$ bar^{-1} h^{-1} at 30 and 50 °C, respectively. All catalysts were found to be electrochemically active in the working potential range of -2 to $+2$ V. A change in the potential of Ni(II) was provoked by the N_4 donor bridging ligands, increasing the ethylene oligomerization activity.

S. Budagumpi · R. P. Johnson · C.-S. Ha · I. Kim (✉)
Department of Polymer Science and Engineering, The WCU Center for Synthetic Polymer Bioconjugate Hybrid Materials, Pusan National University, Busan 609-735, Republic of Korea
e-mail: ilkim@pusan.ac.kr

S. Budagumpi
e-mail: sinu@pusan.ac.kr

R. P. Johnson
e-mail: rpj@pusan.ac.kr

C.-S. Ha
e-mail: csha@pusan.ac.kr

H. Suh
Chemistry Institute for Functional Materials, Pusan National University, Pusan 609-735, Korea
e-mail: hsuh@pusan.ac.kr

Keywords Binuclear · Nickel complexes · Pyrazole ligand · Oligomerization · Transition metal

1 Introduction

Catalysts containing two or more metal centers are frequently employed in the hope of obtaining synergistic effects of the two active metal centers and the possible occurrence of tandem reactions promoted by these two centers [1]. The activity of such compounds depends on the nature of the ligand, the metal, the chelating atoms, and the metal–metal distance, which affect the metal–metal interactions internally. Compounds encompassing a bimetallic core may demonstrate explicit reactivity patterns for the conversion of olefin monomers into oligomers/polymers, which arise from a subtle interplay between the metals and the ligands. Currently, there is great interest in both bridged and non-bridged bimetallic late-first-row transition-metal coordination catalysts for the oligomerization/polymerization of olefins with definite electronic and steric modulations [2–11].

The catalytic oligomerization of ethylene is a major source of higher olefins, which are versatile chemical intermediates for a wide variety of industrial and consumer products. In particular, nickel-based coordination compounds are known to be effective catalysts for a number of important industrial processes. For example, they are used in the production of low-carbon α-olefins, which are used as comonomers for the production of oil additives, fatty acids, sulfur-free fuels, linear low-density polyethylenes, plasticizers, and lubricants. The oxidation state of the nickel ions appears to play a crucial role in the catalytic performance in these reactions. For instance, in the ethylene oligomerization catalyzed by Ni-containing molecular

sieves, it is considered that Ni^{2+} ions in high-coordination unsaturated environments are the active sites [12]. Conversely, there are many arguments supporting the idea that low-valent nickel ions, most likely Ni^{1+} species, are the active sites for ethylene oligomerization [13–15].

Apart from the oxidation state of the nickel ion, the nature of the substituents attached to the ligand core and the oligomerization temperature also play a significant role in the formation of active sites, which is determined by the interplay of catalysts and alkyl-aluminum-based co-catalysts such as ethyl aluminum sesquichloride (EASC) and methyl aluminoxane (MAO). Although it has been reported that many Ni(II) and Co(II) complexes containing *N*,*O*- and *N*,*N*-bidentate ligands are efficient olefin oligomerization/polymerization precatalysts, the catalytic performance of complexes with a bimetallic Ni(II) core for ethylene oligomerization has hardly been studied. Here, we attempt to correlate the oligomerization activities of a series of bridged binuclear Ni(II) catalysts bearing different alkyl and aryl pendent arms as a function of temperature.

2 Experimental

2.1 Materials and Synthesis

All reactions were performed under a purified nitrogen atmosphere using standard Schlenk techniques. Ethylene of polymerization grade (SK Co., Korea) was purified by passing it through columns of Fisher RIDOX^{TM} catalyst and the molecular sieves 5A and 13X. Organic solvents (ethanol, methanol, and diethyl ether) were distilled over CaH_2 and stored over molecular sieves (4A). Toluene was distilled over Na/benzophenone under nitrogen and stored over molecular sieves (4A). All chemicals (1H-pyrazole-3,5-dicarboxylic acid, thionyl chloride, nickel(II) bromide ethylene glycol dimethyl ether ($NiBr_2$·DME), and all amines used in the present study) were purchased from Aldrich Chem. Co. and used without further purification. Unless noted otherwise, all reagents were purchased from commercial sources and used as received.

2.2 Physical Methods

^1H and ^{13}C NMR spectra were recorded in $CDCl_3$ solvent on a Varian Gemini-2000 300-MHz spectrometer at room temperature using tetramethylsilane (TMS) as the internal reference. Analytical thin-layer chromatography (TLC) was carried out using aluminum plates precoated with Merck 0.25-mm silica gel 60F containing the fluorescent indicator UV254. All ligands were purified by using a Combi-Flash (Companion) auto-column machine. Elemental analysis was carried out using a Vario EL analyzer. IR spectra were recorded in a KBr (ligands)/CsI (catalysts) disc matrix using a Shimadzu FTIR spectrometer (IRPrestige-21) in the range 4000–200 cm^{-1}. The electronic spectra of the complexes were recorded on a Shimadzu UV-1650PC spectrophotometer in the range 1000–200 nm. Cyclic voltammetric studies were performed at room temperature in chloroform under O_2-free conditions by using a Kosentech Model CV-104 (S. Korea). Fast atom bombardment mass spectra (FAB-MS) were obtained from the Korea Basic Science Institute on a JEOL JMS AX 505 spectrometer, operated at 3 kV accelerating voltage, equipped with a JEOL MS-FAB 10 D FAB gun operated at a 10 mA emission current, producing a beam of 6 keV xenon. Nitrobenzyl alcohol was used as matrix. Data acquisition and processing were accomplished using JEOL Complement software. Thermogravimetric (TG) and differential thermal analysis (DTA) measurements of the catalysts were recorded on a DuPont 951 thermogravimetric analyzer under a nitrogen atmosphere, keeping the final temperature at 800 °C and using a heating rate of 10 °C min^{-1}. The oligomers were analyzed by gas chromatography (HP6890), performed using a J&W Scientific DB608 column (30 m × 0.53 mm) with a flame ionization detector (FID). The injector and detector temperatures were kept constant at 250 °C. The program set the initial temperature to 30 °C (held for 2 min) and finishing temperature to 250 °C (held for 10 min), with a heating rate of 10 °C min^{-1}.

2.3 Ethylene Oligomerizations

Ethylene oligomerizations were performed at 1.3 bar in a 250-mL round-bottomed flask, kept at constant temperature by a thermostat and equipped with a magnetic stirrer and a thermometer. High-dilution techniques were adopted to reduce the monomer mass-transport effect. After the addition of the catalyst, the reactor was charged with toluene (80 mL) by using a syringe, and immersed in a constant-temperature bath that had previously been set to the desired temperature. When the reactor had equilibrated with the bath temperature, nitrogen gas was removed in vacuum and ethylene was introduced into the reactor. When no more absorption of ethylene into the toluene was observed, the required amount of co-catalyst was injected into the reactor, resulting in the start of oligomerization. The oligomerization rate was determined every 0.01 s from the rate of consumption, measured by a hotwire flow meter (model 5850 D from Brooks Instrument Div.) connected to a personal computer through an A/D converter. The oligomerization was quenched by the addition of methanol containing HCl (5 vol.%) after cooling. The resulting mixture was passed through an alumina column to remove all aluminum-containing species, and the obtained oligomers were analyzed by gas chromatography.

2.4 Preparation of the Ligands

2.4.1 Preparation of 1H-Pyrazole-3,5-bis(isopropyl)carboxamide (HL^1)

1H-Pyrazole-3,5-dicarboxylic acid (1.56 g, 0.01 mol) was heated at reflux with thionyl chloride (10 mL) in a 50-mL Schlenk flask for 4 h at 115 °C under a nitrogen atmosphere. Excess thionyl chloride was doubly trapped under reduced pressure in a Dewar flask kept in liquid nitrogen. The resultant white pasty solid was cooled in an ice bath for 15 min, and an ethanolic solution of isopropyl amine (1.18 g, 0.02 mol) was then added and the mixture was heated at reflux for a further 4 h, whereupon a clear colorless solution was produced. Diethyl ether was added to the obtained reaction mixture, affording a colorless solid (HL^1), which was separated by filtration and purified using hexane ethyl acetate mixture (7:3 v/v). The product was dried in vacuum at room temperature and stored in a vacuum dessicator. The reactions involved in the preparation of the ligands are outlined in Fig. 1. Yield: 68%. Elemental analysis: Found (calculated) for $C_{11}H_{18}N_4O_2$: C 55.2 (55.4), H 7.5 (7.6), N 24.1 (23.5). FTIR (KBr disc) cm^{-1}: 3320 ν(N–H, amide, and pyrazole ring), 2920 ν(C–H, alkyl), 1643 ν(>C=O, amide), 1567 ν(>C=N, pyrazole ring), and 1055 ν(N–N, pyrazole ring). ^{1}H NMR ($CDCl_3$) ppm: 9.2 (s, 1H, pyrazole ring –NH proton), 8.1 (s, 2H, amide protons), 7.0 (s, 1H, pyrazole aromatic proton), 3.1 (sept, 2H, methylene proton), and 0.9 (d, 12H, methyl proton). ^{13}C NMR ($CDCl_3$) ppm: 161 (>C=O, amide), 109, 116 (aromatic pyrazole), 47 (methylene), and 24 (methyl). UV–Vis ($CHCl_3$) nm: 300 (π–π* of C=N) and 311 (n–π* of N and O).

2.4.2 Preparation of 1H-Pyrazole-3,5-bis(diisopropyl)carboxamide (HL^2)

HL^2 was prepared according to the procedure detailed in Sect. 2.4.1, except that diisopropyl amine (2.02 g, 0.02 mol) was added instead of isopropyl amine. Yield: 61%. Elemental analysis: Found (calculated) for $C_{17}H_{30}N_4O_2$: C 63.8 (63.3), H 10.0 (9.4), N 17.1 (17.4). FTIR (KBr disc) cm^{-1}: ≈3300 ν(N–H, pyrazole ring), 2922 ν(C–H, alkyl), 1647 ν(>C=O, amide), 1491 ν(>C=N, pyrazole ring), and ≈1055 ν(N–N, pyrazole ring). ^{1}H NMR ($CDCl_3$) ppm: 11.5 (s, 1H, pyrazole ring –NH proton), 7.9 (s, 1H, pyrazole aromatic proton), 3.3 (sept, 2H, methylene proton), and 1.4 (d, 24H, methyl proton). ^{13}C NMR ($CDCl_3$) ppm: 178 (>C=O, amide), 109, 100 (aromatic pyrazole), 62 (methylene), and 45 (methyl). UV–Vis ($CHCl_3$) nm: 304 (π–π* of C=N) and 312 (n–π* of N and O).

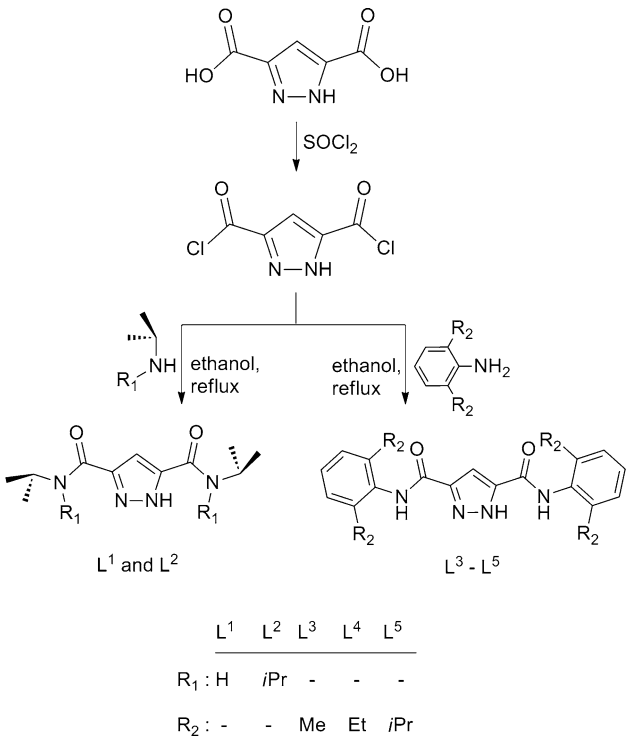

Fig. 1 Synthetic route for the preparation of binucleating ligands

2.4.3 Preparation of 1H-Pyrazole-3,5-bis(2′,6′-dimethylaniline)carboxamide (HL^3)

HL^3 was prepared according to the procedure detailed in Sect. 2.4.1, except that 2,6-dimethyl aniline (2.42 g, 0.02 mol) was added instead of isopropyl amine. Yield: 73.6%. Elemental analysis: Found (calculated) for $C_{21}H_{22}N_4O_2$: C 69.2 (69.6), H 6.5 (6.1), N 14.6 (15.5). FTIR (KBr disc) cm^{-1}: ≈3330 ν(N–H, amide and pyrazole ring) 2922, 2879 ν(C–H, alkyl and aryl), 1648 ν(>C=O, amide), 1533 ν(>C=N, pyrazole ring), and 1044 ν(N–N, pyrazole ring). ^{1}H NMR ($CDCl_3$) ppm: 10.2 (s, 1H, pyrazole ring –NH proton), 9.6 (s, 2H, amide protons), 7.1 (s, 1H, pyrazole aromatic proton), 6.7–7.0 (m, 6H, aromatic), and 2.4 (s, 12H, methyl). ^{13}C NMR ($CDCl_3$) ppm: 138 (>C=O, amide), 131, 129, 118 (aniline aromatic region), 102, 105 (pyrazole aromatic region), and 20 (methyl). UV–Vis ($CHCl_3$) nm: 291 (π–π* of C=N) and 319 (n–π* of N and O).

2.4.4 Preparation of 1H-Pyrazole-3,5-bis(2′,6′-diethylaniline)carboxamide (HL^4)

HL^4 was prepared according to the procedure detailed in Sect. 2.4.1, except that 2,6-diethyl aniline (2.98 g, 0.02 mol) was added instead of isopropyl amine. Yield: 72.1%. Elemental analysis: Found (calculated) for $C_{25}H_{30}N_4O_2$: C 71.2

(71.7), H 8.3 (7.2), N 13.1 (13.4). FTIR (KBr disc) cm^{-1}: 3387 ν(N–H, amide and pyrazole ring), 2916, 2881 ν(C–H, alkyl and aryl), 1635 ν(>C=O, amide), 1458 ν(>C=N, pyrazole ring), and 1047 ν(N–N, pyrazole ring). ^{1}H NMR ($CDCl_3$) ppm: 10.1 (s, 1H, pyrazole ring –NH proton), 7.9 (s, 2H, amide protons), 7.3 (s, 1H, pyrazole aromatic proton), 6.9–7.2 (m, aromatic protons), 2.9 (q, 4H, methylene), and 1.1 (t, 6H, methyl). ^{13}C NMR ($CDCl_3$) ppm: 158 (>C=O, amide), 132, 128, 121 (aniline aromatic region), 100, 97 (pyrazole aromatic region), 36 (methylene), and 23 (methyl). UV–Vis ($CHCl_3$) nm: 303 (π–π* of C=N) and 311 (n–π* of N and O).

2.4.5 *Preparation of 1H-Pyrazole-3,5-bis(2′,6′-diisopropylaniline)carboxamide (HL^5)*

HL^5 was prepared according to the procedure detailed in Sect. 2.4.1, except that 2,6-diisopropyl aniline (3.54 g, 0.02 mol) was added instead of isopropyl amine. Yield: 58.7%. Elemental analysis: Found (calculated) for $C_{29}H_{38}N_4O_2$: C 71.7 (73.4), H 8.5 (8.1), N 9.9 (11.8). FTIR (KBr disc) cm^{-1}: 3375 ν(N–H, amide and pyrazole ring), 2935, 2889 ν(C–H, alkyl and aryl), 1645 ν(>C=O, amide), 1477 ν(>C=N, pyrazole ring), and 1052 ν(N–N, pyrazole ring). ^{1}H NMR ($CDCl_3$) ppm: 11.9 (s, 1H, pyrazole ring –NH proton), 11.2 (s, 2H, amide protons), 7.8 (s, 1H, pyrazole aromatic proton), 7.2–7.6 (m, aromatic protons), 3.1 (sept, 4H, methylene), and 1.1 (d, 24H, methyl). ^{13}C NMR ($CDCl_3$) ppm: 112 (>C=O, amide), 106, 103, 100 (aniline aromatic region), 94, 91 (pyrazole aromatic region), 44 (methylene), and 11 (methyl). UV–Vis ($CHCl_3$) nm: 297 (π–π* of C=N) and 306 (n–π* of N and O).

2.5 Preparation of the Catalysts

For preparing a representative catalyst ($Ni_2L^1Br_3$), a solution of ligand (2 mmol) in methanol (15 mL) was stirred for 30 min, after which a methanolic solution of $NiBr_2$ ethylene glycol dimethyl ether ($NiBr_2$·DME) (4 mmol) was added dropwise over a period of 30 min. The reaction mixture was heated at reflux for 8 h and then cooled to room temperature; the resultant mixture was precipitated in ether and filtered. The filtered solids were washed with methanol and ether to remove traces of metal salt, and they were finally dried and stored in vacuum. Yield: 73.2%. Elemental analysis: Found (calculated) for $C_{11}H_{17}N_4O_2$-Ni_2Br_3: C 23.3 (22.2), H 2.5 (2.9), N 11.1 (9.4). FTIR (KBr disc) cm^{-1}: 3397 ν(N–H, amide), 2986 ν(C–H, alkyl), 1648 ν(>C=O, amide), 1528 ν(>C=N, pyrazole ring), 1405 ν(N–N, pyrazole ring), and 469 ν(M–N). UV–Vis (Toluene) nm: 302 (π–π* of C=N), 310 (n–π* of N and O), and ≈460 (d–d). FAB mass spectrum, *m/z* 513 [M^+ –Br], 353 [M^+ –3Br], 238 [M^+ –Ni_2Br_3].

$Ni_2L^2Br_3$: Yield: 73.2%. Elemental analysis: Found (calculated) for $C_{17}H_{29}N_4O_2Ni_2Br_3$: C 30.5 (30.1), H 4.6 (4.3), N 8.6 (8.3). FTIR (KBr disc) cm^{-1}: 3177 ν(N–H, amide), 3020 ν(C–H, alkyl), 1647 ν(>C=O, amide), 1420 ν(>C=N, pyrazole ring), 1410 ν(N–N, pyrazole ring), and 482 ν(M–N). UV–Vis (Toluene) nm: 308 (π–π* of C=N), ≈320 (n–π* of N and O), and ≈470 (d–d). FAB mass spectrum, *m/z* 597 [M^+ –Br], 322 [M^+ –Ni_2Br_3].

$Ni_2L^3Br_3$: Yield: 73.2%. Elemental analysis: Found (calculated) for $C_{21}H_{21}N_4O_2Ni_2Br_3$: C 35.7 (35.1), H 3.2 (3.0), N 7.6 (7.8). FTIR (KBr disc) cm^{-1}: 3190 ν(N–H, amide), 3006 ν(C–H, alkyl and aryl), 1638 ν(>C=O, amide), 1434 (>C=N, pyrazole ring), 1391 ν(N–N, pyrazole ring), and 456 ν(M–N). UV–Vis (Toluene) nm: 300 (π–π* of C=N), 315 (n–π* of N and O), and ≈460 (d–d). FAB mass spectrum, *m/z* 637 [M^+ –Br], 477 [M^+ –3Br], 362 [M^+ –Ni_2Br_3].

$Ni_2L^4Br_3$: Yield: 73.2%. Elemental analysis: Found (calculated) for $C_{25}H_{29}N_4O_2Ni_2Br_3$: C 40.1 (38.8), H 3.5 (3.8), N 7.6 (7.2). FTIR (KBr disc) cm^{-1}: 3177 ν(N–H, amide), 3012 ν(C–H, alkyl and aryl), 1637 ν(>C=O, amide), 1417 (>C=N, pyrazole ring), 1413 ν(N–N, pyrazole ring), and 455 ν(M–N). UV–Vis (Toluene) nm: ≈325 (π–π* of C=N and n–π* of N and O), and ≈460 (d–d). FAB mass spectrum, *m/z* 693 [M^+ –Br], 534 [M^+ –3Br], 418 [M^+ –Ni_2Br_3].

$Ni_2L^5Br_3$: Yield: 73.2%. Elemental analysis: Found (calculated) for $C_{29}H_{37}N_4O_2Ni_2Br_3$: C 41.2 (41.9), H 4.5 (4.5), N 6.6 (6.7). FTIR (KBr disc) cm^{-1}: 3200 ν(N–H, amide), 2926 ν(C–H, alkyl and aryl), 1642 ν(>C=O, amide), 1472 (>C=N, pyrazole ring), 1355 ν(N–N, pyrazole ring), and 471 ν(M–N). UV–Vis (Toluene) nm: 312 (π–π* of C=N), ≈320 (n–π* of N and O), and ≈470 (d–d). FAB mass spectrum, *m/z* 751 [M^+ –Br], 590 [M^+ –3Br], 474 [M^+ –Ni_2Br_3].

3 Results and Discussion

3.1 General Characterization and Electrochemistry of Ligands and Catalysts

The elemental analyses of all the compounds are consistent with the proposed structures with 2:1 metal–ligand stoichiometry (Fig. 2). All the synthesized compounds are insoluble in water, sparingly soluble in common organic solvents such as hexane, pentane, toluene, and dioxane, and completely soluble in THF, $CHCl_3$, DMF, and DMSO. Except for HL^1, all the compounds are stable and non-hygroscopic at room temperature. Ligand HL^1 is hygroscopic and handled with care in the reactions.

On the basis of a comparison of the IR spectra of the ligands and respective Ni(II) catalysts, it is possible to

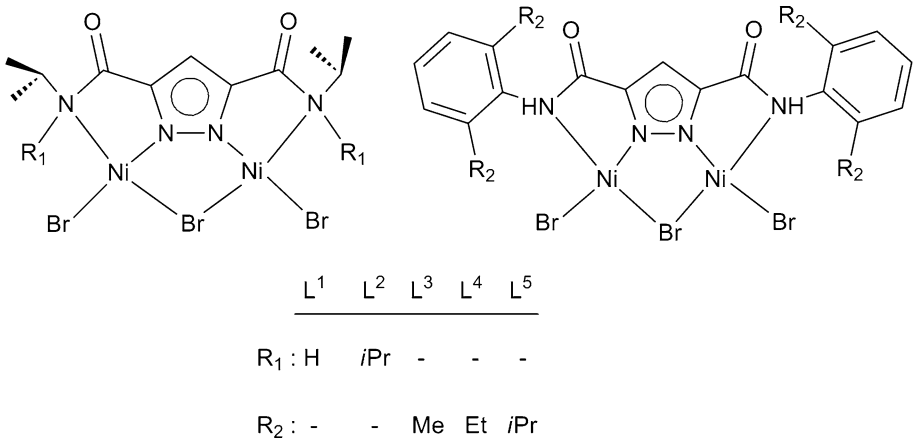

Fig. 2 Proposed structures of the complexes

determine the coordination mode of the ligands. At first glance, all the ligands show characteristic medium-intensity bands in the regions 1643–1651 and 3320–3350 cm^{-1}, which are attributed to amide carbonyl and N–H stretching frequencies, respectively. Upon metallation, the former band is unchanged, whereas the latter is shifted to higher energy by 20–25 cm^{-1}, indicating the involvement of the –NH groups present in the side arms without deprotonation. Another point about the IR spectra that deserves comment is the appearance of pyrazole ring vibrations in the region 1567–1574 cm^{-1}. However, this particular band shifted to a lower-energy region in the catalyst spectra, suggesting the classical endogenous diazine-bridging of the heterocyclic ring system [16, 17]. Two non-ligand bands appeared in all the spectra of the Ni(II) catalysts at around 450–485 and 275 cm^{-1}, because these arise purely from Ni–N and Ni–Br stretching modes [18].

The acquisition of meaningful ^{1}H and ^{13}C NMR spectra of the ligands supports their respective structures. All the ligands show distinguished singlets in their ^{1}H NMR spectra in the regions 9.3–11.2 and 8.5–9.8 ppm, which are ascribed to the resonance of the pyrazole ring –NH and amide protons of the ligands, respectively [19, 20]. The aromatic and methyl/ethyl/isopropyl signals of all the ligands are found in comparable ranges of their ^{1}H and ^{13}C NMR spectra.

The UV–Vis spectra of the free ligands show two sharp discernible bands in the ranges 291–304 and 306–319 nm; these absorptions are consistent with π–π^* and n–π^* transitions arising from the >C=N and N–H functionalities, respectively [21, 22]. The Ni(II) derivatives were also subjected to UV–Vis absorption studies; however, due to their poor solubility in toluene, it was not possible to calculate their molar extension coefficients, so instead, absorption maxima are given at the end of the characterization part for each catalyst. Upon metallation, these bands showed a red shift, indicating the involvement of pyrazolyl diazine (>C=N) and amide nitrogen atoms (N–H) in the coordination. All the Ni(II) catalyst spectra show a d–d transition band in the region 450–515 nm, indicating that the catalysts are four-coordinated Ni(II) systems [21, 22].

Thermogravimetric analysis was carried out on all five catalysts under a nitrogen atmosphere at a heating rate of 10 °C min^{-1}. All the catalysts exhibit similar thermal behavior. The TGA displays two obvious steps in the weight loss of the catalysts. The first corresponds to the loss of three bromide ions (two coordinated and one bridged) as HBr in the range 220–275 °C (the weight loss observed is consistent with the theoretical values). The same is further confirmed by an exothermic DTA signal at around 255 °C in all cases. The second weight loss occurs above 500 °C, and is attributed to the decomposition of the organic part of the catalyst. In the case of $Ni_2L^3Br_3$, an additional weight loss is observed in the range 90–110 °C, which is attributed to the presence of two crystal-held water molecules. Except for $Ni_2L^3Br_3$, all the catalysts appear to have excellent thermal stability, as no clear weight loss is observed below 220 °C.

The molecular weight of the catalysts produced by each ligand was analyzed by FAB mass spectrometry, and the results were found to be consistent with the mass of the catalysts. Furthermore, the fragmentation pattern of the catalysts initially followed the sequential elimination of bromides, then the ligand part.

A number of studies have focused on the electrochemical behavior of metal complexes containing two or more chemically equivalent electroactive sites. For the reversible sequential transfer of two electrons, ΔE_p in the cyclic voltammograms (CVs) would be 42 mV [23]. In contrast, cyclic voltammograms of molecules with multiple, non-interacting redox centers would be similar to those of the corresponding species with a single center, and ΔE_p should be 58 mV [24]. However, the cyclic voltammograms of the present catalysts show no indication of mixed-valence metals. Representative cyclic voltammograms of $Ni_2L^4Br_3$

in DMF solutions are shown in Fig. 3. The CVs of the free ligands and their Ni(II) complexes were measured, scanning between −2 and +2 V at scan rates of 25, 50, 100, 150, 200, 250, and 300 mV min^{-1}. Under similar experimental conditions, electrochemical studies of the free ligand systems using cyclic voltammetry showed no electrochemical activity within the scanned potential window. Therefore, the electrochemical waves observed in the cyclic voltammograms of the catalysts are due purely to the metal.

The CVs of all the catalysts show one-electron quasi-reversible redox behavior for each Ni(II) ion. The oxidation potentials for the Ni(II) catalysts are in the range 50–150 and 950–1100 mV at a scan rate of 25 mV s^{-1}, and shift to higher potentials as the scan rate is increased. Correspondingly, two reduction waves are observed in the reverse scan, which can be attributed to the reduction of one Ni(III) per wave. The reduction potentials are in the region 100–250 and 950–1050 mV at a scan rate of 25 mV s^{-1}, and shift towards more negative potentials with increasing scan rate. Overall, the difference between the anodic and cathodic peak potentials (ΔE_p) is more than 58 mV; hence, the redox system is designated as a one-electron quasi-reversible process for each Ni(II) ion. The redox processes are not coupled with any chemical reaction; this is evident from the E1/2 value that is constant for different scan rates in all the catalyst voltammograms. The oxidation and corresponding reduction reactions obey the diagnostic criteria, i.e., I_{pc}/I_{pa} is almost constant but not unity for a quasi-reversible electron transfer [25]. Assignments for the stepwise nickel-based redox processes of the catalysts are shown below.

$$\text{Oxidation: Ni(II), Ni(II)} - e^- \rightarrow \text{Ni(III), Ni(II)}$$
$$- e^- \rightarrow \text{Ni(III), Ni(III)}$$
$$\text{Reduction: Ni(III), Ni(III)} + e^- \rightarrow \text{Ni(II), Ni(III)}$$
$$+ e^- \rightarrow \text{Ni(II), Ni(II)}$$

Although the chemical environments around the two Ni(II) ions are the same, the overall two-electron exchanges appear as separate one-electron processes, indicating that oxidation/reduction at one site has a steric and electronic influence on the other site, and hence induces a positive/negative shift in the oxidation/reduction potential of the metal ion. This redox mechanism can be explained in terms of the flexibility and size of the coordination cavity in these catalysts, in addition to the geometric requirements and the size of the nickel ions in different oxidation states.

3.2 Analysis of Active Species by the UV–Vis Spectral Technique

Because structurally diverse active species or aluminum intermediates were formed, we contemplated which structural components might be essential for an active Ni(II) species in the olefin oligomerizations in the presence of highly active alkyl aluminum compounds, i.e., EASC. We conducted a thought experiment to identify the Ni(II) active species formed when catalysts interact with a pyrophoric alkyl aluminum compound and those that might be required for a compound to show oligomerization activity and to permit the formation of ethylene oligomers. Absorption spectra of all the Ni(II) catalysts were obtained in the presence of the co-catalyst EASC as a function of

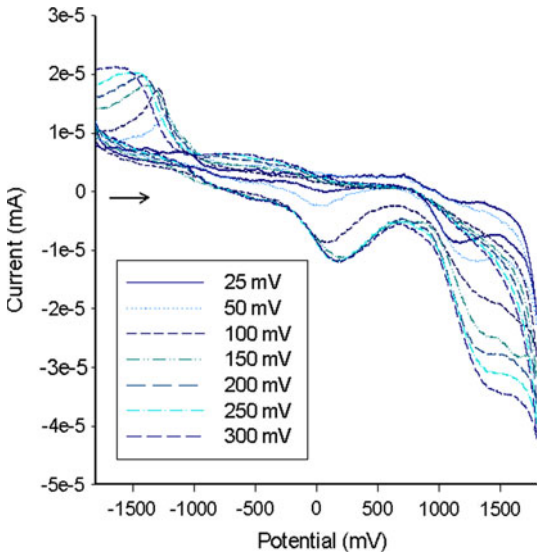

Fig. 3 Cyclic voltammograms of $Ni_2L^4Br_3$ catalyst at different scan rates

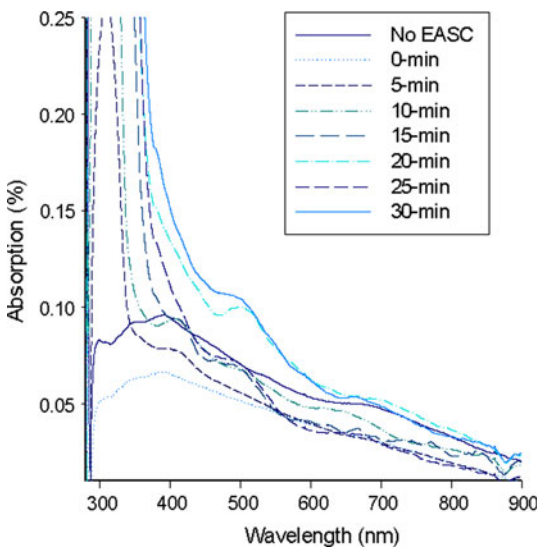

Fig. 4 UV–Vis spectra of $Ni_2L^5Br_3$ in presence of EASC (Ni/Al = 300) and ethylene monomer as a function of time

time under the conditions for ethylene oligomerization; scans were taken before the addition of EASC and every 5 min after EASC addition for 30 min.

In the visible range, the Ni(II) catalyst absorption is very weak between 450 and 485 nm because of its poor solubility in toluene. This could be attributed to the four-coordinated Ni(II) ion under the present ligand field. As soon as EASC is added to the toluene solution of the sparingly soluble Ni(II) catalyst, a vigorous reaction commences and the solution becomes homogeneous. The addition of EASC in an appropriate molecular ratio to the catalyst induces a new d–d transition band; this shifts to lower energy with the formation of a four-coordinated Ni(II) species. A regular shift to lower energy is observed in all the Ni(II) catalysts because of the formation of the ethyl nickel intermediate, in which the ethyl group induces an electropositive character on the metal ion. Between 485 and 515 nm the absorption increases as a function of time, leading to absorption maxima, because of the formation of a greater number of ethyl substituted intermediates as time progresses. Correspondingly, the maxima due to π–π^* and n–π^* transitions also suffer a gradual shift to lower energies because of the formation of ethyl-substituted intermediates. It is pertinent to note the green–black coloration of the reaction medium, followed by the precipitation of black solid particles, and a decrease in the intensity of the band at 485–515 nm. These changes are accompanied by a rapid deactivation of the catalytic system [26–28]. Simultaneously, a band appears in the region 700–720 nm, which is due to the formation of the active species. The UV–Vis spectra of $Ni_2L^5Br_3$ in the presence of EASC (Ni/Al 300:1) and ethylene as a function of time are shown in Fig. 4. On the basis of this, it can be assumed that the four-coordinated active species is formed during the oligomerization, and is responsible for the formation of the obtained oligomers with defined yield.

Table 1 Results of ethylene oligomerizations by $Ni_2L^{1-5}Br_3$ catalysts combined with ethyl aluminum sesquichloride (EASC)

Entry	Catalyst	Temp. (°C)	R_p[a] × 10^{-6}	Distribution of olefins[b] (%)				
				C4	α-C4	C6	C8	C10
1	$Ni_2L^1Br_3$	30	0.66	95.9	2.0	4.1	0.0	0.0
2	$Ni_2L^2Br_3$	30	0.75	79.9	50.8	7.4	5.7	7.0
3	$Ni_2L^3Br_3$	30	1.02	44.3	0.0	50.3	3.9	1.5
4	$Ni_2L^4Br_3$	30	1.22	68.1	13.4	25.4	4.4	2.0
5	$Ni_2L^5Br_3$	30	1.24	78.5	12.8	11.3	6.1	4.0
6	$Ni_2L^1Br_3$	50	0.32	79.6	18.9	12.4	4.3	3.7
7	$Ni_2L^2Br_3$	50	0.40	77.1	78.1	17.2	3.0	2.7
8	$Ni_2L^3Br_3$	50	0.48	93.3	8.8	0.8	3.4	2.5
9	$Ni_2L^4Br_3$	50	0.49	93.2	13.3	2.0	1.9	2.9
10	$Ni_2L^5Br_3$	50	0.45	88.3	3.6	3.7	4.1	3.9

Conditions: catalyst = 5 μmol, [EASC]/[Ni] = 300, toluene = 80 mL, $P_{C_2H_4}$ = 1.3 bar, and reaction time = 30 min

[a] Rate of polymerization over a polymerization period in g (mol-Ni)$^{-1}$ bar^{-1} h^{-1}

[b] Determined by GC analysis

All our attempts to carry out similar characterizations of the Ni(II) active species formed during oligomerization using cyclic voltammetric techniques were unsuccessful because of the deposition of solid samples on the electrodes.

3.3 Ethylene Oligomerizations

The catalyst activity is comparable to some Ni(II) coordination catalysts with N-donor ligands under similar conditions. Previously, Brookhart reported that catalysts with only one substituent on the N-ring for the α-diimine do not yield polymers but instead produce oligomers [29]. The products are mainly butenes and hexenes, with small/

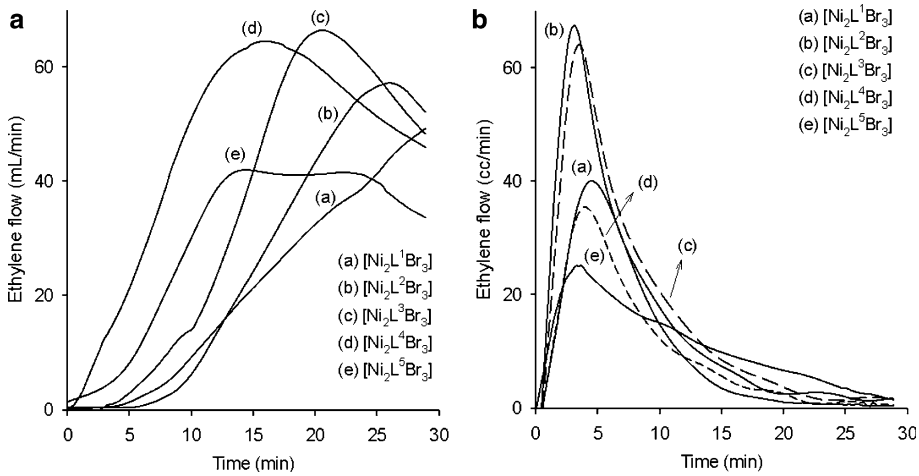

Fig. 5 Ethylene consumption rate curves of $Ni_2L^{1-5}Br_3$ catalysts at 30 °C (**a**) and 50 °C (**b**). Oligomerization conditions: catalyst = 5 μmol, [EASC]/[Ni] = 300, toluene = 80 mL, $P_{C_2H_4}$ = 1.3 bar, and reaction time = 30 min

moderate amounts of higher oligomers up to C10. Similar outcomes have been reported in many studies involving atom-bridged active bimetallic cores for olefin oligomerizations [3, 30, 31]. The oligomer distribution pattern is consistent with a nickel hydride species being the active center, where fast elimination of β-hydride limits the products to mostly butenes and hexanes; however, in a few cases higher olefins are also observed in trace amounts. For these binuclear nickel systems, a coordination–insertion mechanism seems likely, followed by β-hydride elimination (chain transfer) [29].

After combination of the Ni(II) catalysts with EASC, we found them all to be highly active in ethylene oligomerizations under the given conditions (Fig. 5; Table 1). In order to increase the oligomerization activity of the catalysts, the ligand design was tuned sterically in a significant way to produce the desired products. The effects of various steric substituents on the catalysts' activities were investigated by simple *ortho* substitution of the aromatic amine ligand. The overall activities of all the catalysts at 30 and 50 °C were compared (Table 1). The catalysts oligomerize the ethylene into C4, C6, C8, and C10 fractions with activities up to 1.2 and 0.5 $\times$ 10^6 g(mol-Ni)$^{-1}$ bar^{-1} h^{-1} at 30 and 50 °C, respectively (Fig. 5a, b). The mechanism of oligomerization is depicted in Fig. 6. When chain transfer occurs from species V/VI, only α-olefins can be produced. Internal olefins (2-alkenes) can be produced only when chain transfer occurs from secondary alkyl agnostic species VII after consuming an ethylene molecule [32].

Catalyst systems composed of electron-deficient nickel centers such as $Ni_2L^2Br_3$ (compared with other aliphatic amine ligands) and $Ni_2L^5Br_3$ (compared with other

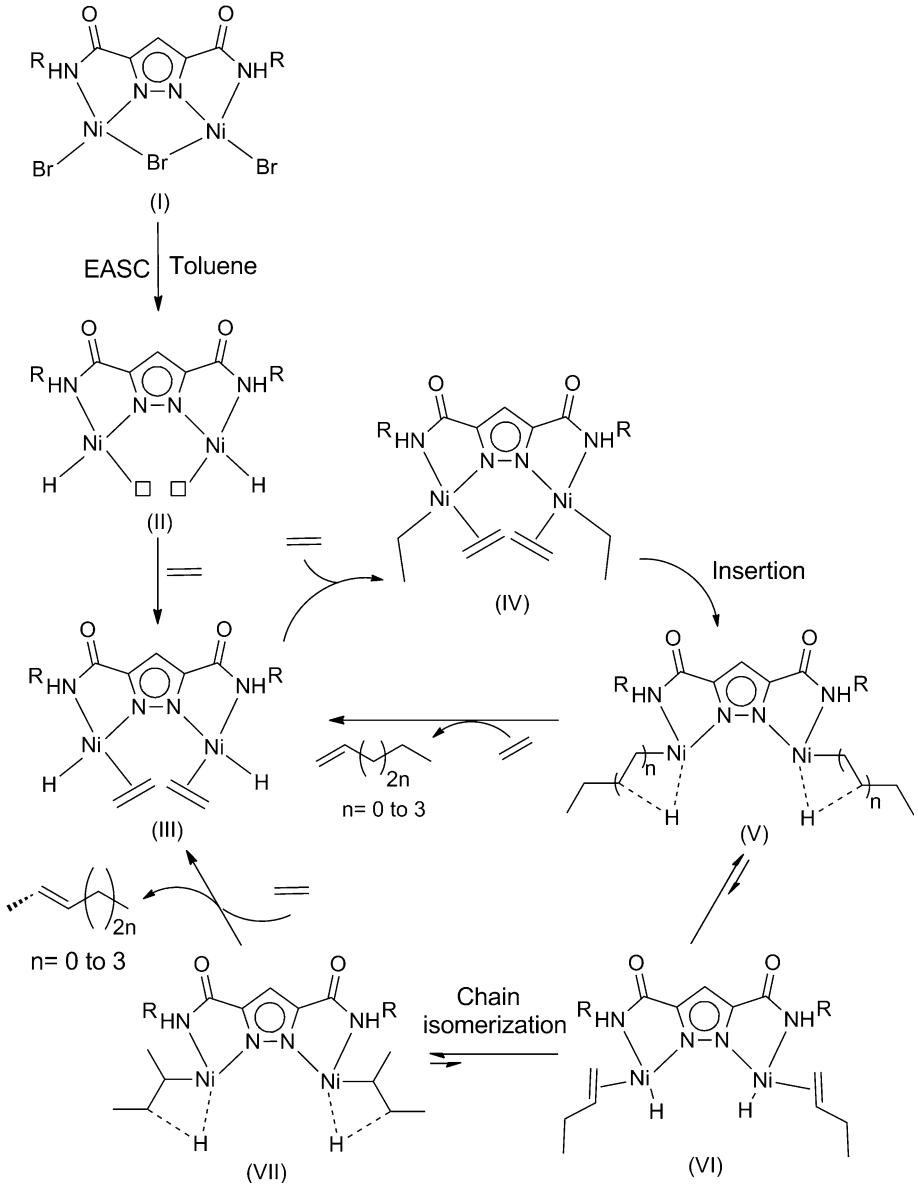

Fig. 6 Proposed mechanism for ethylene oligomerization by diazene bridged Ni(II) catalysts combined with EASC

aromatic amine ligands) were found to be the most active, while catalyst activity was found to be lower in relatively electron-rich metal centers such as $Ni_2L^1Br_3$, $Ni_2L^3Br_3$, and $Ni_2L^4Br_3$. However, the catalyst $Ni_2L^2Br_3$ showed remarkable activity towards the conversion of ethylene, especially to the α-C4 fraction, and produced 50.84 and 76.44% of the α-C4 fraction out of its 751.4 and 403.5 kg mol^{-1} yields at 30 and 50 °C, respectively. The catalysts $Ni_2L^3Br_3$ and $Ni_2L^4Br_3$ revealed that the reduction of steric methyl/ethyl at the *ortho*-aryl position resulted in a decrease in their activities, and the steric environment around the central metal affected their catalytic activities because of the relatively poorer electron-donor methyl/ethyl substituents compared to the isopropyl group. In the case of the catalysts derived from aliphatic amines, $Ni_2L^2Br_3$ bears two additional isopropyl groups on either side of the tetratopic ligand, which increase the electron deficiency on the nickel center, ultimately causing a higher yield of oligomers at both the temperatures used. These results are rather better than those reported for bridged binuclear catalysts in the literature [3].

4 Conclusions

In this article, we have presented the synthesis and spectroscopic and structural characterization of a new family of pyrazole-scaffold-based binuclear Ni(II) complexes suitable for ethylene oligomerizations into C4, C6, C8, and C10 fractions, with activities up to 1.2 and 0.5×10^6 g(mol-Ni)$^{-1}$ bar^{-1} h^{-1} at 30 and 50 °C, respectively. The ligands in the present study were synthesized by the action of 3,5-dichloroformyl-1H-pyrazole on aliphatic and aromatic primary/secondary amines under anhydrous conditions. Indeed, N_2-coordination of the heterocyclic ring to the Ni(II) ions offers an exceptional opportunity to develop and increase the scope of diazine-bridged binuclear Ni(II) complexes. Moreover, it has been shown that heterocyclic diazine-bridged Ni(II) complexes can also serve as ethylene oligomerizing agents, in which the two metal centers are connected by a pyrazolyl-diazine module. The electrochemical study of the catalysts using cyclic voltammetry in dimethyl formamide at a concentration of 10^{-3} M indicated the quasi-reversible one-electron redox behavior of each Ni(II) ion. It is assumed that the change in the potential of Ni(II) is provoked by the bridging ligands, increasing the ethylene oligomerization activity.

Acknowledgment We thank the World Class University Program (No. R32-2008-000-10174-0) and Brain Korea-21 (BK-21) for grants that supported this work.

References

1. Takeuchi D (2010) Dalton Trans 39:311
2. Tomov A, Kurtev A (1995) J Mol Catal A Chem 103:95
3. Champouret YDM, Fawcett J, Nodes WJ, Singh K, Solan GA (2006) Inorg Chem 45:9890
4. Dohler T, Helmar G, Walther D (2000) Chem Commun 945
5. Li L, Metz MV, Li H, Chen M-C, Marks TJ, Liable-Sands L, Rheingold AL (2002) J Am Chem Soc 124:12725
6. Li H, Marks TJ (2006) Proc Natl Acad Sci USA 103:15295
7. Zhang S, Vystorop I, Tang Z, Sun W-H (2007) Organometallics 26:2456
8. Zhang S, Sun W-H, Kuang X, Vystorop I, Yi J (2007) J Organomet Chem 692:5307
9. Guo N, Stern CL, Marks TJ (2008) J Am Chem Soc 130:2246
10. Rodriguez BA, Delferro M, Marks TJ (2009) J Am Chem Soc 131:5902
11. Coffin RC, Schneider Y, Kramer EJ, Bazan GC (2010) J Am Chem Soc 132:13869
12. Wendt G, Finster J, Schoellner R, Siegel H (1981) Stud Surf Sci Catal 7:978
13. Davydov AA, Kantcheva M, Chepotko M (2001) Catal Lett 83:97
14. Lallemand M, Finiels A, Fajula F, Hulea V (2009) J Phys Chem C 113:20360
15. Sohn JR, Park WC, Park SE (2002) Catal Lett 84:259
16. Saha NC, Saha A, Butcher RJ, Chaudhuri S, Saha N (2002) Inorganica Chim Acta 39:348
17. Saha NC, Butcher RJ, Chaudhuri S, Saha N (2003) Polyhedron 22:375
18. Sau DK, Butcher RJ, Chaudhuri S, Saha N (2004) Polyhedron 23:5
19. Anna KD, El·zbieta M, Barbara R, Izabela DA, Anna EK, Malgorzata AB (2007) Chem Pharm Bull 55:747
20. Mazurek W, Bond HM, Murray KS, O'Conner MJ, Weed AG (1985) Inorg Chem 24:2484
21. West DX, Nassar AA (1999) Transition Met Chem 24:617
22. Lever ABP (1968) Inorganic electronic spectroscopy. Elsevier, Amsterdam
23. Polycn DS, Shain I (1966) Anal Chem 38:370
24. Flanagam JB, Bard AJ, Anson FC (1978) J Am Chem Soc 100:4248
25. Gomes L, Pereira E, Castro BD (2000) Dalton Trans 1373
26. Bijal KB, Son GW, Park D-W, Ha C-S, Kim I (2008) J Polym Sci A Polym Chem 46:1066
27. Peruch F, Cramail H, Deffieux A (1999) Macromolecules 32:7977
28. Chandran D, Kwak CH, Oh JM, Ahn IY, Ha C-S, Kim I (2008) Catal Lett 125:27
29. Svejda SA, Brookhart M (1999) Organometallics 18:65
30. Kunrath F, De Souza RF, Casagrande OL Jr, Brooks NR, Young VJ Jr (2003) Organometallics 22:4739
31. Jie S, Zhang D, Zhang T, Sun W-H, Chen J, Ren Q, Liu D, Zheng G, Chen W (2005) J Organomet Chem 690:1739
32. Rodriguez BA, Delferro M, Marks TJ (2008) Organometallics 27:2166